Sub-cellular origin of mtDNA deletions in human skeletal muscle

Running head: Pathogenesis of mtDNA deletion clonal expansion

Amy E Vincent PhD[1], Hannah S Rosa PhD[1], Kamil Pabis MRes[1], Conor Lawless PhD[1], Chun Chen MBBS MRes[1], Anne Grünewald PhD[1-3], Karolina A Rygiel PhD[1], Mariana C Rocha PhD[1], Amy K Reeve PhD[1], Gavin Falkous[1], Valentina Perissi PhD[4], Kathryn White PhD[5], Tracey Davey[5], Basil J Petrof MD FRCP[6], Avan A Sayer PhD FRCP[7], Cyrus Cooper DM FRCP[8], David Deehan MD FRCS[9], Robert W Taylor PhD FRCPath[1], Doug M Turnbull PhD FRCP [1], Martin Picard PhD[10,11,12]

[1] Wellcome Centre for Mitochondrial Research and Newcastle Centre for Ageing and Vitality, Institute of Neurosciences, Newcastle University, Newcastle upon Tyne, UK

[2] Institute of Neurogenetics, University of Lübeck, Lübeck, Germany

[3] Molecular and Functional Neurobiology Group, Luxembourg Centre for Systems Biomedicine, University of Luxembourg, Esch-sur-Alzette, Luxembourg, Luxembourg

[4] Department of Biochemistry, Boston University School of Medicine, Boston, MA, USA

[5] EM Research Services, Newcastle University, Newcastle upon Tyne, UK

[6] Meakins-Christie Laboratories, Department of Medicine, McGill University Health Centre, Montréal, Canada

[7] NIHR Newcastle Biomedical Research Centre, Newcastle upon Tyne Hospitals NHS Foundation Trust and Newcastle University, UK

[8] MRC Lifecourse Epidemiology Unit, University of Southampton, UK

[9] Institute of Cellular Medicine, Newcastle University, United Kingdom

[10] Department of Psychiatry, Division of Behavioral Medicine, Columbia University Medical Center, New York, NY, USA

[11] Department of Neurology and Columbia Translational Neuroscience Initiative, H. Houston Merritt Center, Columbia University Medical Center, New York, NY, USA

[12] Columbia University Aging Center, Columbia University, New York, NY USA

Contact: doug.turnbull@ncl.ac.uk; martin.picard@columbia.edu

Abstract

OBJECTIVE: In patients with mtDNA maintenance disorders mtDNA deletions sporadically form and clonally expand within individual muscle fibers, causing respiratory chain deficiency. This study aimed to investigate the first visible sign of respiratory chain deficiency.

This article has been accepted for publication and undergone full peer review but has not been through the copyediting, typesetting, pagination and proofreading process, which may lead to differences between this version and the Version of Record. Please cite this article as doi: 10.1002/ana.25288

METHODS: Serial skeletal muscle cryosections from patients with multiple mitochondrial DNA deletions were subjected to subcellular immunofluorescent, histochemical and genetic analysis.

RESULTS: We report respiratory chain deficient perinuclear foci containing mtDNA deletions, which show local elevations of both mitochondrial mass and mtDNA copy number. These subcellular foci of respiratory chain deficiency are associated with a local increase in mitochondrial biogenesis and unfolded protein response (UPR^{mt}) signaling pathways. We also find that the commonly reported pattern of segmental mitochondrial deficiency is consistent with the three-dimensional organization of the mitochondrial network.

INTERPRETATION: We propose that mtDNA deletions first exceed the biochemical threshold causing biochemical deficiency in focal regions adjacent to the myonuclei, before spreading across the muscle fiber. These sub-cellular resolution data provide new insights into the possible origin of mitochondrial respiratory chain deficiency in mitochondrial myopathy.

Keywords: clonal expansion; mitochondrial genome; skeletal muscle;

INTRODUCTION

Nuclear-encoded mutations affecting the replication and maintenance of the mitochondrial genome (mtDNA) are a common cause of mitochondrial disease[1], typically causing multiple mtDNA deletions. Due to the polyploid nature of mtDNA in individual cells, mtDNA deletions must clonally expand to high levels before they cause respiratory deficiency. The clinical phenotype for these disorders is variable, ranging from isolated progressive external ophthalmoplegia (PEO) to PEO with additional symptoms including proximal myopathy, ataxia, sensory axonal neuropathy and optic atrophy. Genes associated with these phenotypes encode proteins involved in mtDNA replication (e.g. *POLG* and *TWNK, DNA2, MGME1*), dNTP supply (e.g. *TP, RRM2B, TK2, DGUOK*), and proteins regulating mitochondrial dynamics (*OPA1* and *MFN2*)[2].

Clonal expansion of mtDNA deletions is an important cause of mitochondrial respiratory chain deficiency. A critical unanswered question is where and how, within the cell cytoplasm new mtDNA deletions expand from a single mutated mtDNA molecule to become the dominant mtDNA species. Several theoretical models have been proposed to explain the clonal expansion of mutant mtDNA[3-8]. However, previous models were based on cell populations *in vitro*[9, 10] or invertebrate models with pre-existing mixtures of mutant mtDNA[11, 12].

Skeletal muscle fibers have a highly organized cytoarchitecture, where spatially-restricted mitochondrial subpopulations exist[13, 14]. Subsarcolemmal (SS) mitochondria are located at the periphery of the muscle fiber adjacent to the sarcolemma membrane, a subset of which are perinuclear intermyofibrillar (IMF) mitochondria are located between the myofibrils at the z-band.

This raises the question, how does clonal expansion proceed through these highly organized and spatially restricted mitochondrial populations? To investigate this process, we sought to localize and analyze the earliest biochemical defect in muscle fibers from patients. We hypothesis that, increasing our understanding of this phenomena will provide insight into

the origins of mtDNA deletions and respiratory chain deficiency, with potential diagnostic and prognostic implications.

EXPERIMENTAL PROCEDURES

Muscle biopsies

Muscle biopsies from Quadriceps were obtained via needle biopsy under local anaesthetic. Ethical approval was granted by the Newcastle and North Tyneside Local Research Ethics Committees (reference 2002/205) and prior informed consent was obtained from each participant. Normal human ageing samples were obtained from the Hertfordshire cohort[15]. Control tissue (n = 20) was acquired with prior informed consent from people undergoing anterior cruciate ligament surgery, following approval by Newcastle and North Tyneside Local Research Ethics Committees (reference 12/NE/0395). All experiments were carried out in accordance with the approved guidelines. Muscle samples were frozen in liquid N_2-cooled isopentane, mounted on in OCT and stored at -80°C until use, or fixed for electron microscopy.

All biopsies from mtDNA maintenance disorders (n = 7) had confirmed genetic diagnoses. COX/SDH histochemistry was used to screen biopsy specimens and those with a suitable muscle histology and a significant degree (>2-5%) of cytochrome c oxidase (COX) deficiency (COX-SDH+) were included (Supplementary Table 1). Patient selection for each experiment was based on tissue availability due to the large number of sections required for each experiment. Genetic and immunofluorescent analysis were completed on separate sections due to the need for high contrast in a single image for accuracy with laser capture microdissection.

COX/SDH histochemistry

To quantify the prevalence of COX-deficient foci, cryosectioned muscle (10µm) from transversely orientated muscle blocks, from mtDNA maintenance disorder patients (n = 6, patients 1-4, 6 and 7), was subjected to sequential COX/SDH histochemistry[16] and independently analysed by two investigators. Strict criteria were applied for foci

quantification. Only circumscribed foci deficient in COX activity but with SDH activity (i.e. COX-SDH+), that were localised in an otherwise COX-positive fibre were counted as a COX-deficient niche.

COX/SDH and nuclear staining

Serial 8µm sections were subject to COX/SDH histochemistry before counterstaining with DAPI (Sigma D9542) (2µg/ml) for 5 minutes and mounting in ProLong Gold (Thermofisher P10144). Images were captured in both brightfield and DAPI channels individually and merged. At least 14 serial sections were reconstructed to provide three-dimensional information about the length of COX-deficient foci and their proximity to myonuclei.

mtDNA deletion and copy number analysis

Serial muscle sections (15µm) treated for COX/SDH histochemistry were cryosectioned on to PEN membrane slides (Zeiss, #000635-17). Patient selection for genetic analysis was based on tissue availability. Muscle fibers with regions of focal cross-sectional COX-deficiency were identified and the COX-deficient area was laser microdissected and captured into separate 0.2ml tubes using a PALM system (Zeiss). Two identically sized subsarcolemmal regions from the remainder of the muscle fiber were also captured along with –whole COX-positive and COX-deficient muscle fibers as controls. Muscle fibers were captured into 15µl single-cell lysis buffer (0.5M Tris-HCl, 0.5% Tween 20, 1% Proteinase K, pH 8.5) and incubated at 55°C for 3 hours followed by 10 minutes at 95°C. The lysate was then diluted 1:5 and analysed in triplicate using a D-Loop/*MT-ND1*/*MT-ND4* triplex real-time PCR deletion assay[17]. A serial dilution of the p7D1 plasmid was used to generate a standard curve from each plate. In order for a plate of samples to be included in analyses, an amplification efficiency of 100-95% was required for the standard curve. Major arc deletions were quantified by computing the ratio of *MT-ND1*/*MT-ND4*. Negative values arising from this assay, which may result from deletion of *MT-ND1*, are shown as zero.

Due to the low mtDNA content of the foci and of the similarly sized COX-positive regions of the muscle fiber, we further implemented a stringent quality control threshold requiring all foci and corresponding regions of the same fiber to be at least three quantification cycle (Cq) values below the no-template control for *MT-ND1*. The D-Loop region can become triple-stranded during transcription/replication[18], so analysis of D-Loop/*MT-ND1* ratios in cells that did not have deletions encompassing *MT-ND1* were used to exclude this possibility. As a control, two to four fully COX-deficient and COX-positive control fibers were also run in triplicate on every plate.

By these criteria, ~68% of cells were eliminated due to inadequate amplification. Overall, 27 foci and their matched COX-positive regions from five patients with *POLG* (n = 2), *RRM2B* (n = 2) and *TWNK* (n = 1) mutations (patients 2-5 and 7, Supplementary Table 1) showed robust amplification and were used for subsequent analyses.

Immunofluorescence

Serial cryosections (8µm) were subject to quantitative immunofluorescence staining[19]. Antibodies used include: anti-MTCOI (Abcam ab14705), anti-SDHA (Abcam ab14715), anti-laminin (Sigma L9393), IgG2a-488 (S-21131), anti-rabbit-405 (A-31556), biotinylated IgG1 (S32357) and streptavidin-647 (S21374, all from Life Technologies). Following the secondary antibody incubation, sections were washed and counterstained with DAPI (2µg/ml) for 5 minutes and mounted in ProLong Gold. Sections were imaged on a Zeiss Axio imager M1 microscope equipped with a motorized stage using multidimensional acquisition tiling in ZEN (Zeiss, blue edition).

SDHA expression was correlated with porin (VDAC1), a known indicator of mitochondrial mass[19], with significant concordant SDHA/Porin levels indicating that SDHA is a viable mitochondrial mass marker (Fig 2F).

Image analysis

The average fluorescent intensity corresponding to the abundance of an investigated protein in the muscle fibers was quantified using Image J (version 1.50i) or IMARIS v.7.7.2

(Bitplane)[19, 20]. The “plot profile” functions in Image J and ZEN (blue edition) were used to compare changes in MTCOI and SDHA abundance across muscle fibers, subtracting the background fluorescence for each channel.

Immunofluorescent assessment of signaling molecules

Antibodies against PGC1α (Millipore Ab3243), TFAM (Abcam Ab119684), NEF2L2 (Abcam ab31163), ClpP (Sigma HPA010649), Htra2 (R&D Systems AF1458), mtHsp70 (Thermofisher), Hsp60 (BD Transduction Systems 611562), GPS2 [21], p62 (Progen GP62-C), Beclin1 (Millipore Ab15417), Pink1 (Abcam Ab23707), LC3-II (cell signaling 4108) and Parkin (Santa Cruz biotechnologies sc-32282) to assess signaling, were used in combination with MTCOI, SDHA and DAPI to assess changes with COX-deficiency in a single section of muscle. Antibodies that did not produce a sufficient signal-to-noise ratio, or were highly correlated with mitochondrial mass, were removed from further analysis. TFAM, Hsp60, GPS2 and Beclin1 were selected for immunofluorescence on serial sections (n = 4) of patients with multiple mtDNA deletions (n = 3, patients 4, 5 and 7, Supplementary Table 1). IMARIS v.7.7.2 (bitplane) was used to assess average fluorescent intensity of TFAM and Hsp60 relative to MTCOI/SDHA ratio in whole COX-positive and COX-deficient fibers. Subsequently average intensity of the foci was compared to a COX-positive region of the fiber.

Fiber section perimeter profiling to identify perinuclear regions and regions of mitochondrial deficiency

Serial skeletal muscle sections were labelled for MTCOI, SDHA and DAPI (as described above) from three patients with multiple mtDNA deletions (patients 3, 5 and 7, Supplementary Table 1). A total of 74 fibers containing foci of mitochondrial deficiency were identified by visual inspection and used for fiber section perimeter profiling (Fig 4D). DAPI, SDHA and MTCOI fluorescence intensity profiles were constructed (Fig 4E). Differences in DAPI intensities between sections were reduced by subtracting the background intensity (modal, unsaturated DAPI intensity) of each section. Perinuclear perimeter segments were

identified as those with a corrected DAPI intensity greater than the 0.85 quantile of corrected intensity observed in all 74 fibers across serial sections in three patients. All points along intensity profiles were manually annotated as COX-positive or COX-deficient by visual inspection of perimeter profiles as well as linear line scans through the centre of the muscle fiber to identify perimeter segments with mitochondrial deficiency.

Predicted and observed levels of focus-perinuclear overlap

For each section, we measured the fraction of the perimeter annotated as perinuclear (P), the fraction of the perimeter annotated as focal (F) and the fraction of the perimeter annotated as focus-perinuclear overlap (O). We also calculated the fraction of the perimeter which we would expect to be annotated as focus-perinucleus overlap if the location of the perinuclear region and nuclei were un-related and random (Overlap predicted (O_{pred}), Fig 4F). According to the specific multiplication rule for the probability of two independent events co-occurring, we would expect that:

$$O_{pred} = P \times F$$

To test if differences between O_{pred} and Observed (O) were significant, a one-tailed t-test to examine whether O_{pred} - O was significantly different from zero was performed (Fig 4F). Code and data underlying profiling and overlap analysis can be found at https://github.com/lwlss/MitoDysfunctionFoci.

Serial block face scanning electron microscopy (SBF-SEM)

As described previously, serial block face-scanning electron microscopy sample preparation and imaging was performed[22] to examine mitochondrial organization. Four muscle fibers from 12 muscle biopsies were imaged and assessed, representative images are shown in Fig 6D.

Statistics

A combination of two-tailed unpaired (whole muscle fibers) and paired (matched sub-cellular regions) t tests were used. Statistical significance was set at 0.05. Data for focal

regions of deficiency are either presented as individual COX-deficient fiber regions with paired COX-positive regions. All analyses were performed in Prism v7.0 (Graph Pad).

RESULTS

Foci of respiratory chain deficiency are a pathological hallmark of mtDNA deletions

We investigated skeletal muscle biopsies from patients with multiple mtDNA deletions due to nuclear gene mutations affecting mtDNA maintenance (n = 7) (Supplementary Table 1, Fig 1). The commonly reported pattern of respiratory chain deficiency in skeletal muscle consists of a mosaic pattern of COX-positive and COX-deficient muscle fibers, with the affected muscle fibers observed in the longitudinal orientation harboring confined segments of respiratory chain deficiency[3, 23-26] (Fig 1A).

As expected, we observed COX-deficient muscle fibers in both the transverse and longitudinal orientations (Figs 1A and 1B). In addition, we identified focal regions of respiratory chain deficiency within individual muscle fibers (Fig 1C-D). These foci were observed in patients with mitochondrial disease and normal muscle biopsies of older individuals, but not in age-matched control biopsies (n = 20).

To estimate the prevalence of COX-deficient foci in specific mtDNA maintenance disorders we surveyed cryosections reacted for sequential COX/SDH histochemistry from patients with *TWNK*, *RRM2B* and *POLG* mutations (n = 6, patients 1-4, 6 and 7). A total of 11 COX-deficient foci and 929 fully COX-deficient muscle fibers were identified (Fig 1E). Skeletal muscle biopsies contained on average 11.9% (range 0.8 - 30.5%) fully COX-deficient muscle fibers, compared to 0.15% (range 0 - 0.33%) with restricted COX-deficient foci (Fig 1E). The total prevalence of COX-deficient foci relative to total muscle fibers and fully COX-deficient muscle fibers was estimated at 1:571 and 1:58, respectively.

Focal regions of deficiency are restricted to the subsarcolemmal space

When surveying COX/SDH histochemistry, we consistently found that focal regions of deficiency are localized in the subsarcolemmal space (Fig 1B-D). This finding was corroborated by quantitative immunofluorescence[19](Fig 2). We generated MTCOI/SDHA intensity profiles to map the distribution of COX deficiency with sub-cellular resolution. The spectrum of MTCOI deficiency ranged from confined perinuclear foci (Fig 2B), to segmental and completely MTCOI-deficient muscle fibers (Fig 2C and 2D). Furthermore, comparing SDHA fluorescent intensity in COX-deficient foci and COX-positive regions of the same fibers indicated that SDHA protein abundance was consistently higher by an average of 3.3-fold in MTCOI-deficient foci (Fig 2E), indicating a local increase of mitochondrial mass specifically in areas of respiratory chain deficiency.

We verified that this increase in SDHA protein was specific to COX-deficient niches, and not a result of increased mitochondrial content near the nucleus (i.e., perinuclear vs subsarcolemmal), by analysis of normal muscle fibers from patients and controls (data not shown). The use of SDHA as a mitochondrial mass marker was validated against VDAC1 (Fig 2F), showing that both markers yield equivalent results.

Respiratory-deficient foci contain mtDNA deletions

We next confirmed that respiratory chain-deficient foci contain higher levels of mtDNA deletions than the rest of the muscle fiber, using laser capture microdissection (LCM) of small sub-cellular areas followed by triplex real time PCR (Fig 3). This analysis was performed in patients with mutations in mtDNA maintenance genes *POLG or RRM2B* (Patients 2, 3, 4, 5 and 7). COX-deficient foci and two identically sized COX-positive areas of the same muscle fiber were microdissected (Fig 3A).

The majority of COX-deficient foci had deletions encompassing *MT-ND4*, and some deletions encompassing *MT-ND1*, whereas COX-positive areas of the same muscle fiber generally only contained normal mtDNA, or lower levels of the deletion (Fig 3B). On average, significantly higher mtDNA deletion levels were detected in foci compared to COX-positive regions (Fig 3B, right). Less than 10% of fibers had deletions encompassing *MT-ND1* (not

shown), consistent with previous findings[27]. The same deletion pattern was observed in whole fibers (Fig 3E).

mtDNA copy number and mitochondrial mass is increased in COX- foci

If increased mitochondrial biogenesis contributed to the accumulation of deleted mtDNA molecules, we reasoned that mtDNA copy number should similarly be elevated in the respiratory chain-deficient foci compared to COX-positive regions of the same cell. Therefore, we measured absolute mtDNA copy number density in COX-deficient foci relative to corresponding COX-positive regions of the same fibers, using an optimized standard curve method (Fig 3E)[17]. Since *MT-ND4*, and occasionally *MT-ND1* can both be deleted in human skeletal muscle[27], we used *D-Loop* and *MT-ND1* amplicons as metrics of copy number.

Consistent with the elevation in mitochondrial protein content (Fig 2E), mtDNA copy number was increased in the majority of COX-deficient foci (Fig 3C). Isolated COX-deficient foci relative to COX-positive regions showed a mean 2.2-fold higher (range 1.1 – 9.6, $p < 0.001$) *D-Loop* copy number (Fig 3C). This was confirmed by *MT-ND1* copy number, where the within-fiber difference between COX-deficient and COX-positive regions was 2.5-fold (range 1.1 – 11.7, $p < 0.001$) (Fig 3D). In comparison, cells with complete COX deficiency showed on average a 1.9-fold (range 1.0 – 6.5, $p = 0.03$) higher *D-Loop* copy number, and 1.9-fold (range 1.0 – 6.2, $p = 0.03$) higher *MT-ND1* copy number (Fig 3E) compared to cells with normal COX activity. Thus, COX-deficient foci are associated with local upregulation of mtDNA copy number.

Accumulation of COX-deficient mitochondrial mass occurs near myonuclei

Mitochondrial biogenesis is dependent on several nuclear encoded proteins, therefore we hypothesized that the localization of COX-deficient mutant niches in the subsarcolemmal space may be due to the presence of myonuclei. Thus, serial 8µm sections were subjected to COX/SDH histochemistry counter-stained with DAPI to determine the focal

distribution and topology of COX-deficient foci in relation to the myonuclei along the length of muscle fibers (Fig 4A). Immunofluorescent labelling of serial sections for MTCOI/SDHA/DAPI further confirmed the co-localization of COX-deficient niches with myonuclei (Fig 4B-4C).

To identify COX-deficient foci that did not co-localize with nuclei, we profiled perinuclear regions and MTCOI fluorescent intensity along the perimeters of fiber sections containing a region of COX deficiency. Perinuclear regions were identified automatically by thresholding DAPI signal along the perimeter. Focal regions of COX deficiency were manually classified by visual inspection of SDHA and MTCOI profiles along the perimeter (Fig 4D and E) and by line scan quantification as in Fig 2. Across 74 fiber sections containing COX-deficient foci, 26.2% of the perimeter was classified as perinuclear and 20.0% was classified as COX-deficient foci. Given the relative proportions of perinuclear space and focal deficiency, if the location of nuclei and COX-deficient foci were un-related (i.e., random), we would expect only 5.23% of the perimeter to be classified as overlap. In contrast, 9.5% was classified as COX-deficient foci and perinuclear overlap. To determine the significance of this difference, in each muscle fiber the observed overlap was measured and the predicted foci-nuclei overlap calculated.

The differences between predicted and observed overlap fractions were found to be significantly lower than zero (p = 4.26e^{-15}, Fig 4F and G). A total of 75 distinct foci were identified in 74 cells, all of which at least partially overlapped with a perinuclear region, consistent with the required presence of a nucleus for clonal expansion of mutant mitochondria.

Localized activation of mito-nuclear signaling pathways with mtDNA deletions

To assess if signaling may be contributing to the increased mitochondrial content and mtDNA deletions in the perinuclear niche, we probed markers of i) mitochondrial biogenesis, ii) UPR^{mt} and iii) mitophagy (Fig 5A). We analyzed the mitochondrial biogenesis marker TFAM, UPR^{mt} marker Hsp60, retrograde signaling factor GPS2[28] and mitophagy marker Beclin1 (Fig 5A). COX-deficient foci were compared to equivalent COX-positive regions of

the same fibers, representing the early stage respiratory chain deficiency (Fig 5B) and fully COX-deficient fibers compared to COX-positive fibers representing the late-stage of respiratory chain deficiency (Fig 5C).

Relative to COX-positive regions of individual muscle fibers, Hsp60 and GPS2 were both higher in focal regions of deficiency in 89.6% and 86.2% of foci, respectively (Fig 5B). Both the UPR^{mt} and GPS2 retrograde signaling pathways have been shown to be upstream of mitochondrial biogenesis[12, 28]. Accordingly, mitochondrial TFAM was also increased in 70% of foci, relative to COX-positive regions. In fully COX-deficient fibers, Hsp60 and GPS2 were also significantly increased, relative to COX-positive fibers (Fig 5C). TFAM was significantly elevated in fully COX-deficient fibers, consistent with the overall increase in mtDNA copy number in late-stage COX-deficient fibers.

In addition, we also analyzed COX-positive perinuclear regions from COX-positive fibers of patients and controls, which were compared to subsarcolemmal but non-perinuclear regions to rule out a potential non-specific elevation of markers throughout the SS region. We found that Hsp60 and TFAM levels were similar, however GPS2 was elevated in perinuclear regions, consistent with its role as nuclear transcription factor[28]. In patient muscle, compared to perinuclear COX-positive areas, Hsp60 (2.2-fold), GPS2 (1.2-fold), and TFAM (1.5-fold) levels were all higher in COX-deficient niches.

A reduction in quality control processes to remove mutant mitochondria via autophagy could also have contributed to the accumulation of mutant mitochondria in specific sub-cellular compartments. Immunolabelling of the autophagic regulator Beclin1[29] showed that levels were unchanged in COX-deficient foci, although significantly higher in fully COX-deficient fibers (Fig 5B and C), with no difference between the subsarcolemmal and intermyofibrillar region.

Respiratory chain deficiency first spreads in cross-section following mitochondrial network anisotropy

Finally, we sought to address whether mitochondrial morphology may dictate the segmental appearance respiratory chain deficiency (Fig 6A). Examining muscle fibers longitudinally revealed the existence of short COX-deficient muscle fiber segments, where the diameter of the COX-deficient muscle fibers is substantially wider than the longitudinal axis (Fig 6B). This is supportive of the mitochondrial network model (Fig 6A).

In skeletal muscle cells, intermyofibrillar mitochondria organized at the Z-bands show a substantial degree of branching. We examined the three dimensional morphology of skeletal muscle mitochondria in humans controls (n = 8) and patients (n = 6) using SBF-SEM (Fig 6C and D). Controls and patients both demonstrate high mitochondrial connectivity across the transverse muscle fiber and low connectivity between Z-bands along the muscle fiber, representative images are shown in Fig 6D. These results support the mitochondrial network model and likely provide the structural basis for the segmental COX deficiency that is regularly observed in mitochondrial myopathy[30].

Foci are observed in ageing and other neuromuscular conditions

In addition, to mtDNA maintenance disorders, we sought to determine if foci of deficiency were observed in other myopathies in which *de novo* mtDNA deletions and COX deficiency are found. Foci of COX deficiency were also identified in cases of single, large-scale mtDNA deletions (Fig 7A), inclusion body myositis (IBM) (Fig 7B) and mechanically-ventilated diaphragm (Fig 7C) where COX deficiency is associated with mtDNA deletions[26]. Furthermore, muscle from healthy adults 68-77 years of age also demonstrated COX-deficient foci (n = 79, Fig 7D), which suggested that–the observation is not specific to mitochondrial myopathy but may be relevant to other age-related myopathic conditions.

DISCUSSION

Mitochondrial respiratory chain deficiency in mtDNA maintenance disorders is dependent on the progressive accumulation of mtDNA deletions. Several theories have been

proposed to explain the clonal expansion of mtDNA deletions[4-7]. However, a number of questions remain: In post-mitotic muscle fibers, where do mtDNA deletions originate? How do deleted mtDNA molecules accumulate to higher levels than wild-type mtDNA? What dictates the directional spread of respiratory chain-deficient segments along muscle fibers?

To explore these questions, we performed in-depth imaging and molecular studies of skeletal muscle biopsies from patients with genetically confirmed mtDNA maintenance disorders. We targeted the smallest portion of the muscle fiber presenting with COX deficiency and found that these areas were perinuclear. In addition, we have shown that there is accumulation of mtDNA deletions in the COX-deficient foci and that there is corresponding increase in nuclear-mitochondrial signaling. Therefore, we propose that mtDNA deletions arise and accumulate within the perinuclear mitochondria, where nuclear proximity of mtDNA deletions is a key factor for clonal expansion.

Nuclear proximity as a determining factor in focal COX deficiency

Three factors could contribute to observed mtDNA deletions and respiratory chain deficiency of perinuclear mitochondria: i) increased mutation rate in the perinuclear area, ii) higher replication rates in the perinuclear area, or iii) proximity to the nucleus for retrograde mito-nuclear signaling. Davis and Clayton[31] have previously demonstrated that mtDNA replication rate is higher in the perinuclear region compared to the rest of the cell, consistent with the requirement of nuclear gene products for mitochondrial biogenesis.

In patients harboring mutations in nuclear DNA genes encoding mtDNA replication machinery, a higher local replication rate could account for a higher mutation rate in the perinuclear mitochondria. Thus, it is also possible that there may be multiple deletion species competing within a focus and that the chance of mtDNA deletions being replicated in the perinuclear region may also be higher, due to the higher replication rate.

Furthermore, our data demonstrate that focal regions of COX deficiency have elevated mitochondrial mass and mtDNA copy number concomitant with higher levels of

mito-nuclear signaling molecules, indicative of mitochondrial biogenesis through mito-nuclear "retrograde" signaling. In contrast, we did not find evidence of a change in mitophagy based on Beclin1.

In *Caenorhabditis elegans*, mtDNA deletions trigger nuclear activation of the unfolded protein response (UPR^{mt}) to promote mitochondrial biogenesis and mitochondrial dynamics[11, 12]. With mtDNA deletions existing throughout the worm from birth, this process may increase mtDNA heteroplasmy[11, 12]. The UPR^{mt} has also been shown to modulate both biogenesis and mitophagy levels[11, 12]. Therefore, given the observations in *C. elegans* it is possible that the UPR^{mt} in foci of human muscle may be linked with activation of mitochondrial biogenesis.

Our data in human skeletal muscle suggests a role for the UPR^{mt} and possibly implicates other factors such as GPS2, which transcriptionally activates mitochondrial biogenesis in response to mitochondrial stress or depolarization[32]. Beclin1 labelling suggests no change in mitophagy in small foci. However, Beclin1 may not reflect all mitophagy pathways but is the only target for which antibodies of sufficient quality for frozen muscle samples were available. Based on the differential upregulation of signaling factors in focal COX-deficient and fully COX-deficient fibres, it may be that multiple signaling pathways are activated in different fibers. Clinically-meaningful models will be required to generate mechanistic data and fully resolve these questions.

Focal deficiency, clonal expansion and mitochondrial disease progression

As well as a pathological feature of mtDNA maintenance disorders, focal regions of deficiency were also observed in muscle from patients with single, large-scale mtDNA deletions, and in normal ageing. Segmental respiratory chain deficiency in longitudinal muscle fibers is a pathological hallmark of mitochondrial myopathy and ageing[3, 24, 30]. To our knowledge, this is the first study to report circumscribed cytoplasmic areas of COX deficiency smaller than the diameter of muscle fibers. Our data also demonstrates that, in a muscle section, foci are relatively infrequent compared to fully COX-deficient muscle fibers. Furthermore, although COX-deficient segments in longitudinal orientation have been known

to vary greatly in length, we have documented examples where segments are substantially shorter than the width of the muscle fiber (Fig 6B).

Applying SBF-SEM analysis for the first time in human muscle confirmed the substantially more elaborate nature of the mitochondrial network along z-bands (i.e., I-band mitochondria[33]) in the transverse orientation of human muscle fibers, compared to sparse longitudinal interconnections between sarcomeric planes (Fig 6D). This is in contrast to the almost continuous mitochondrial network previously reported in mice[33]. Thus, because contiguous mitochondria can exchange (mutant) mtDNA through fusion, the anisotropic nature of the human mitochondrial network may account for COX-deficient segments which appear restricted along the length of affected muscle fibers.

Conclusions and proposed model

Based on our observations we propose the following model: mtDNA deletions that arise in the perinuclear region preferentially accumulate under the influence of mitochondrial biogenesis, reaching critical mass and causing the first visible signs of focal mitochondrial respiratory chain deficiency. Mutant mitochondria then preferentially propagate transversely via direct physical interactions between mitochondria, driven in part by increased mitochondrial biogenesis. The clonal nature of these deletions and the role replication plays in this process remain to be investigated. This hypothesis assumes that fully COX-deficient cells (which must have a point of origin) are derived from the spread of small perinuclear foci, but this remains to be established in a model that which can be evaluated overtime.

Acknowledgments

We are grateful to Dr Gavin Hudson for proofreading the final version of this manuscript and to Professor Robert Lightowlers and Dr. Oliver Russell for advice in the validation of the real time PCR assay with Rho0 cells. This work was supported by grants The Wellcome Centre for Mitochondrial Research (203105/Z/16/Z), The MRC Centre for Translational Research in Neuromuscular Disease Mitochondrial Disease Patient Cohort G0800674, the UK NIHR Biomedical Research Centre in Age and Age Related Diseases award to the Newcastle upon Tyne Hospitals NHS Foundation Trust, the MRC/EPSRC Molecular Pathology Node, The Lily Foundation and the UK NHS Specialist Commissioners "Rare Mitochondrial Disorders of Adults and Children" Service. AEV was funded by an MRC studentship (MR/K501074/1) as part of the MRC Centre for Neuromuscular disease (MR/K000608/1) and is now funded by the MRC as part of the Centre for Ageing and Vitality (MR/L016354/1). AG is the recipient of an ATTRACT career development grant from the National Research Fund of Luxembourg (FNR). HSR was supported by The Barbour Foundation. MP is supported by the Wharton Fund and NIH grant R35GM119793. AKR is supported by a senior Parkinson's UK fellowship (F-1401).

Potential conflict of interests:

The authors declare no conflict of interests.

Author contributions:

AEV, MP and DMT contributed to the conception and design of the study. AEV, HSR, KP, CL, ChCh, AG, KW, TD, KAR, MCR, AKR, RWT, VP, BJP, AAS and CyCo contributed to acquisition of data and data analysis. AEV, HSR, CL, MP, DMT contributed to writing of the manuscript**.**

References

1. Gorman GS, Schaefer AM, Ng Y, et al. Prevalence of nuclear and mitochondrial DNA mutations related to adult mitochondrial disease. Ann Neurol. 2015 May;77(5):753-9.
2. Viscomi C, Zeviani M. MtDNA-maintenance defects: syndromes and genes. Journal of inherited metabolic disease. 2017 Jul;40(4):587-99.
3. Campbell G, Krishnan KJ, Deschauer M, Taylor RW, Turnbull DM. Dissecting the mechanisms underlying the accumulation of mitochondrial DNA deletions in human skeletal muscle. Human molecular genetics. 2014 Sep 1;23(17):4612-20.
4. de Grey AD. A proposed refinement of the mitochondrial free radical theory of aging. BioEssays : news and reviews in molecular, cellular and developmental biology. 1997 Feb;19(2):161-6.
5. Elson JL, Samuels DC, Turnbull DM, Chinnery PF. Random intracellular drift explains the clonal expansion of mitochondrial DNA mutations with age. American journal of human genetics. 2001 Mar;68(3):802-6.
6. Kowald A, Kirkwood TB. Transcription could be the key to the selection advantage of mitochondrial deletion mutants in aging. Proceedings of the National Academy of Sciences of the United States of America. 2014 Feb 25;111(8):2972-7.
7. Wallace DC. Mitochondrial DNA mutations and neuromuscular disease. Trends in genetics : TIG. 1989 Jan;5(1):9-13.
8. Fukui H, Moraes CT. Mechanisms of formation and accumulation of mitochondrial DNA deletions in aging neurons. Human molecular genetics. 2009;18(6):1028-36.
9. Diaz F, Bayona-Bafaluy MP, Rana M, Mora M, Hao H, Moraes CT. Human mitochondrial DNA with large deletions repopulates organelles faster than full-length genomes under relaxed copy number control. Nucleic Acids Res. 2002 Nov 01;30(21):4626-33.
10. Hayashi J, Ohta S, Kikuchi A, Takemitsu M, Goto Y, Nonaka I. Introduction of disease-related mitochondrial DNA deletions into HeLa cells lacking mitochondrial DNA results in mitochondrial dysfunction. Proceedings of the National Academy of Sciences of the United States of America. 1991 Dec 01;88(23):10614-8.
11. Gitschlag BL, Kirby CS, Samuels DC, Gangula RD, Mallal SA, Patel MR. Homeostatic Responses Regulate Selfish Mitochondrial Genome Dynamics in C. elegans. Cell Metab. 2016 Jul 12;24(1):91-103.
12. Lin YF, Schulz AM, Pellegrino MW, Lu Y, Shaham S, Haynes CM. Maintenance and propagation of a deleterious mitochondrial genome by the mitochondrial unfolded protein response. Nature. 2016 May 19;533(7603):416-9.
13. Glancy B, Hsu LY, Dao L, et al. In Vivo microscopy reveals extensive embedding of capillaries within the sarcolemma of skeletal muscle fibers. Microcirculation. 2014;21(2):131-47.
14. Picard M, White K, Turnbull DM. Mitochondrial morphology, topology, and membrane interactions in skeletal muscle: a quantitative three-dimensional electron microscopy study. Journal of applied physiology. 2013 Jan 15;114(2):161-71.
15. Syddall HE, Aihie Sayer A, Dennison EM, Martin HJ, Barker DJ, Cooper C. Cohort profile: the Hertfordshire cohort study. International journal of epidemiology. 2005 Dec;34(6):1234-42.
16. Murphy JL, Ratnaike TE, Shang E, et al. Cytochrome c oxidase-intermediate fibres: importance in understanding the pathogenesis and treatment of mitochondrial myopathy. Neuromuscular disorders : NMD. 2012 Aug;22(8):690-8.
17. Rygiel KA, Grady JP, Taylor RW, Tuppen HA, Turnbull DM. Triplex real-time PCR--an improved method to detect a wide spectrum of mitochondrial DNA deletions in single cells. Scientific reports. 2015;5:9906.
18. Kasamatsu H, Robberson DL, Vinograd J. A novel closed-circular mitochondrial DNA with properties of a replicating intermediate. Proceedings of the National Academy of Sciences of the United States of America. 1971 Sep;68(9):2252-7.
19. Rocha MC, Grady JP, Grunewald A, et al. A novel immunofluorescent assay to investigate oxidative phosphorylation deficiency in mitochondrial myopathy: understanding mechanisms and improving diagnosis. Scientific reports. 2015;5:15037.

20. Grünewald A, Rygiel KA, Hepplewhite PD, Morris CM, Picard M, Turnbull DM. Mitochondrial DNA Depletion in Respiratory Chain–Deficient Parkinson Disease Neurons. Annals of Neurology. 2016;79(3):366-78.
21. Cederquist CT, Lentucci C, Martinez-Calejman C, et al. Systemic insulin sensitivity is regulated by GPS2 inhibition of AKT ubiquitination and activation in adipose tissue. Molecular Metabolism. 2017;6(1):125-37.
22. Vincent AE, Ng YS, White K, et al. The Spectrum of Mitochondrial Ultrastructural Defects in Mitochondrial Myopathy. Scientific reports. 2016 08/10/online;6:30610.
23. Matsuoka T, Goto Y, Hasegawa H, Nonaka I. Segmental cytochrome c-oxidase deficiency in CPEO: teased muscle fiber analysis. Muscle Nerve. 1992 Feb;15(2):209-13.
24. Bua E, Johnson J, Herbst A, et al. Mitochondrial DNA-deletion mutations accumulate intracellularly to detrimental levels in aged human skeletal muscle fibers. American journal of human genetics. 2006 Sep;79(3):469-80.
25. Elson JL, Samuels DC, Johnson MA, Turnbull DM, Chinnery PF. The length of cytochrome c oxidase-negative segments in muscle fibres in patients with mtDNA myopathy. Neuromuscular disorders : NMD. 2002 Nov;12(9):858-64.
26. Picard M, Jung B, Liang F, et al. Mitochondrial dysfunction and lipid accumulation in the human diaphragm during mechanical ventilation. American journal of respiratory and critical care medicine. 2012 Dec 1;186(11):1140-9.
27. Rygiel KA, Tuppen HA, Grady JP, et al. Complex mitochondrial DNA rearrangements in individual cells from patients with sporadic inclusion body myositis. Nucleic Acids Res. 2016 Apr 30.
28. Cardamone MD, Tanasa B, Cederquist CT, et al. GPS2 regulates mitochondrial biogenesis via mitochondria retrograde signaling and modulation of nuclear-encoded mitochondrial genes core promoter accessibility. The FASEB Journal. 2017 April 1, 2017;31(1 Supplement):755.15.
29. Margariti A, Li H, Chen T, et al. XBP1 mRNA splicing triggers an autophagic response in endothelial cells through BECLIN-1 transcriptional activation. The Journal of biological chemistry. 2013 Jan 11;288(2):859-72.
30. Shoubridge EA, Karpati G, Hastings KE. Deletion mutants are functionally dominant over wild-type mitochondrial genomes in skeletal muscle fiber segments in mitochondrial disease. Cell. 1990 Jul 13;62(1):43-9.
31. Davis AF, Clayton DA. In situ localization of mitochondrial DNA replication in intact mammalian cells. J Cell Biol. 1996 Nov;135(4):883-93.
32. Cardamone MD, Tanasa B, Cederquist C, et al. GPS2 regulates mitochondria biogenesis via mitochondrial retrograde signaling and chromatin remodeling of nuclear-encoded mitochondrial genes. bioRxiv. 2017.
33. Glancy B, Hartnell LM, Malide D, et al. Mitochondrial reticulum for cellular energy distribution in muscle. Nature. 2015 Jul 30;523(7562):617-20.

Figure Legends:

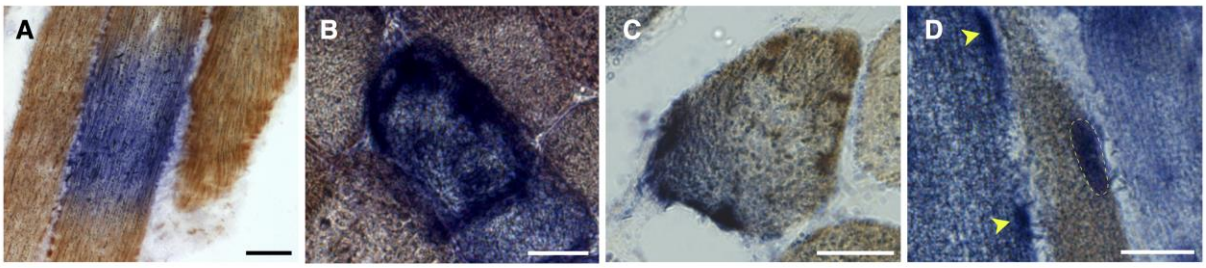

E

		Count			Percentage		
Patient	Geneotype	COX-deficient foci	COX-deficient fiber	Total muscle fibres	% COX-deficient foci	% COX-deficient fiber	% Other fibers
P1	*TWNK*	0	40	469	0.00	8.53	91.47
P2	*RRM2B*	8	392	2421	0.03	16.19	83.48
P3	*RRM2B*	4	148	2615	0.02	5.66	94.19
P4	*RRM2B*	1	219	719	0.01	30.46	69.40
P6	*TWNK*	2	13	1658	0.01	0.78	99.10
P7	*POLG*	2	119	1251	0.02	9.51	90.33

Figure 1. Sub-cellular localization of respiratory chain dysfunction in human skeletal muscle

(A) Three skeletal muscle fibers in longitudinal orientation from cryosections subjected to cytochrome c oxidase (COX, brown) and succinate dehydrogenase (SDH, blue) histochemistry to measure COX and SDH activity. The central fiber has segmental COX deficiency, indicative of segmental mtDNA defects.

(B) Skeletal muscle fiber in cross-sectional (i.e., transverse) orientation which is deficient for COX activity and positive for SDH activity.

(C) Focal segment deficient for COX activity but positive for SDH activity in cross-section orientation.

(D) In longitudinal orientation, focal region deficient for COX activity and positive for SDH activity in a case of multiple mtDNA deletions. Note the restricted nature of COX deficiency consistent with a perinuclear region (dotted line), and the subsarcolemmal increase in SDH activity in an adjacent COX-deficient fiber (arrowheads).

(E) Summary of quantitative analysis of foci frequency in mtDNA maintenance disorders (n = 6). Count data for total, COX-deficient SDH positive fibers (COX-deficient fiber) and COX-deficient foci is presented for each case followed by a percentage of fibers classified as COX-deficient fiber, COX-deficient foci or other (COX-positive or intermediate COX deficiency).

Scale bars, 25 μm.

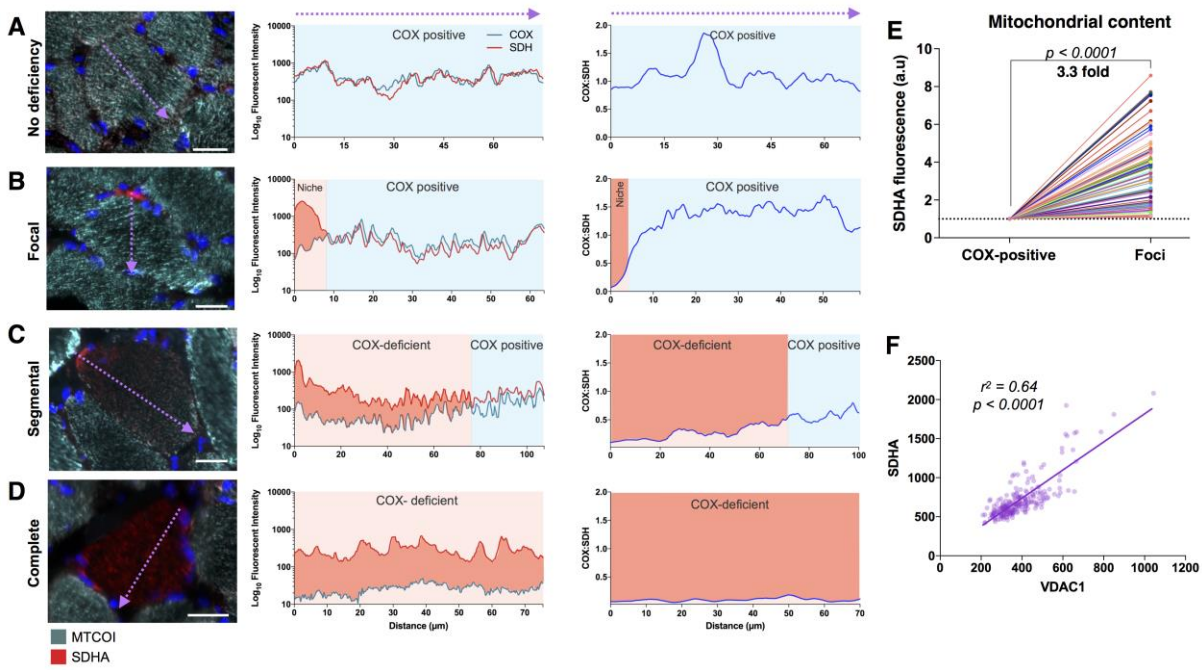

Figure 2. Foci distribution of COX deficiency and mitochondrial content by immunofluorescence in human muscle fibers

(A) MTCOI (green), SDHA (red) and nuclei (blue) immunofluorescent labelling and quantification of a normal COX-positive skeletal muscle fiber (patient 7, *POLG*) (left) corresponding fluorescence intensity plot along the profile denoted by the arrow (middle), and COX:SDH ratio (right).

(B) Muscle fiber (patient 7, *POLG*) with a niche of focal COX deficiency denoted in red in fluorescence intensity plots.

(C) Muscle fiber (patient 7, *POLG*) with segmental COX negativity spread through approximately 70% of the cell's longest diameter.

(D) Muscle fiber (patient 7, *POLG*) with complete COX negativity.

(E) Quantification of mitochondrial content based on SDHA fluorescence intensity in COX-deficient foci and in matched COX-positive subsarcolemmal regions within individual muscle fibers. Data is combined from patients 3 (*RRM2B*), 5 (*POLG*) and 7 (*POLG*). Data is plotted for each cell relative to COX-positive areas (n = 74, two-tailed paired t-test, $p < 0.0001$).

(F) When SDHA and VDAC1 (porin) are plotted against each other for a sample of muscle fibers the regression line has an $r^2 = 0.644$ and $p < 0.0001$.

Scale bars, 25 µm.

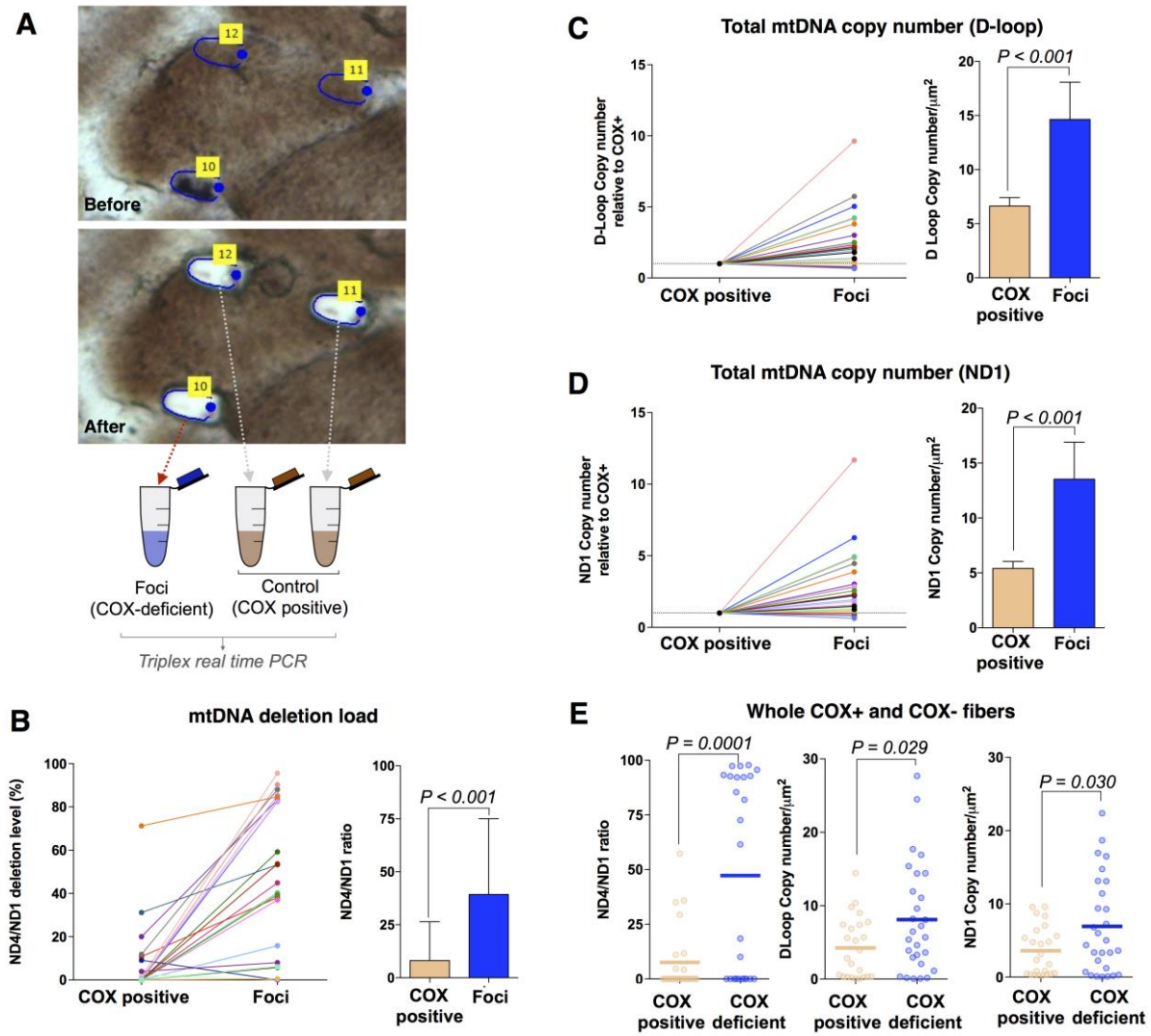

Figure 3. COX-deficient (COX-) foci contain high levels of mtDNA deletions and show compensatory increase in mtDNA copy number

Subcellular and single cell mtDNA analysis was performed on patients with mutations in *POLG* (n = 2), *RRM2B* (n = 2) and *TWNK* (n = 1), patients 2-5 and 7.

(A) Single muscle fiber before and after laser microdissection of one COX- and two COX-positive (COX+) control sub cellular regions.

(B) ND4/ND1 ratio as an indicator of mtDNA deletion level in COX-deficient foci with matched COX-positive sub-cellular regions from single fibers (left), and mean deletion level ± SEM (right).

(C) Total D-Loop mtDNA copy number in COX-deficient foci and matched COX-positive sub-cellular regions from single fibers. Copy numbers are shown relative to COX-positive regions of the same muscle fiber (left) and average copy number by group (right). Mean copy number ± SEM (right).

(D) The same as (C) but with ND1 as the copy number metric.

(E) mtDNA ND4/ND1 ratio, total D-Loop (centre) and total ND1 (right) mtDNA copy number in COX-deficient and COX-positive whole fibers isolated by laser capture microdissection and assessed using real-time PCR. A value of 0 indicates no ND4 deletion, whereas a value of 100 indicates all mtDNA molecules contain a ND4 deletion (left). Each datapoint corresponds to a single fiber. Bars indicate mean values.

Matched sub-cellular regions in (B), (C) and (D) are connected by a matched-colored line. Data are means ± SEM. n = 27 fibers, 5 patients, two-tailed paired t-tests.

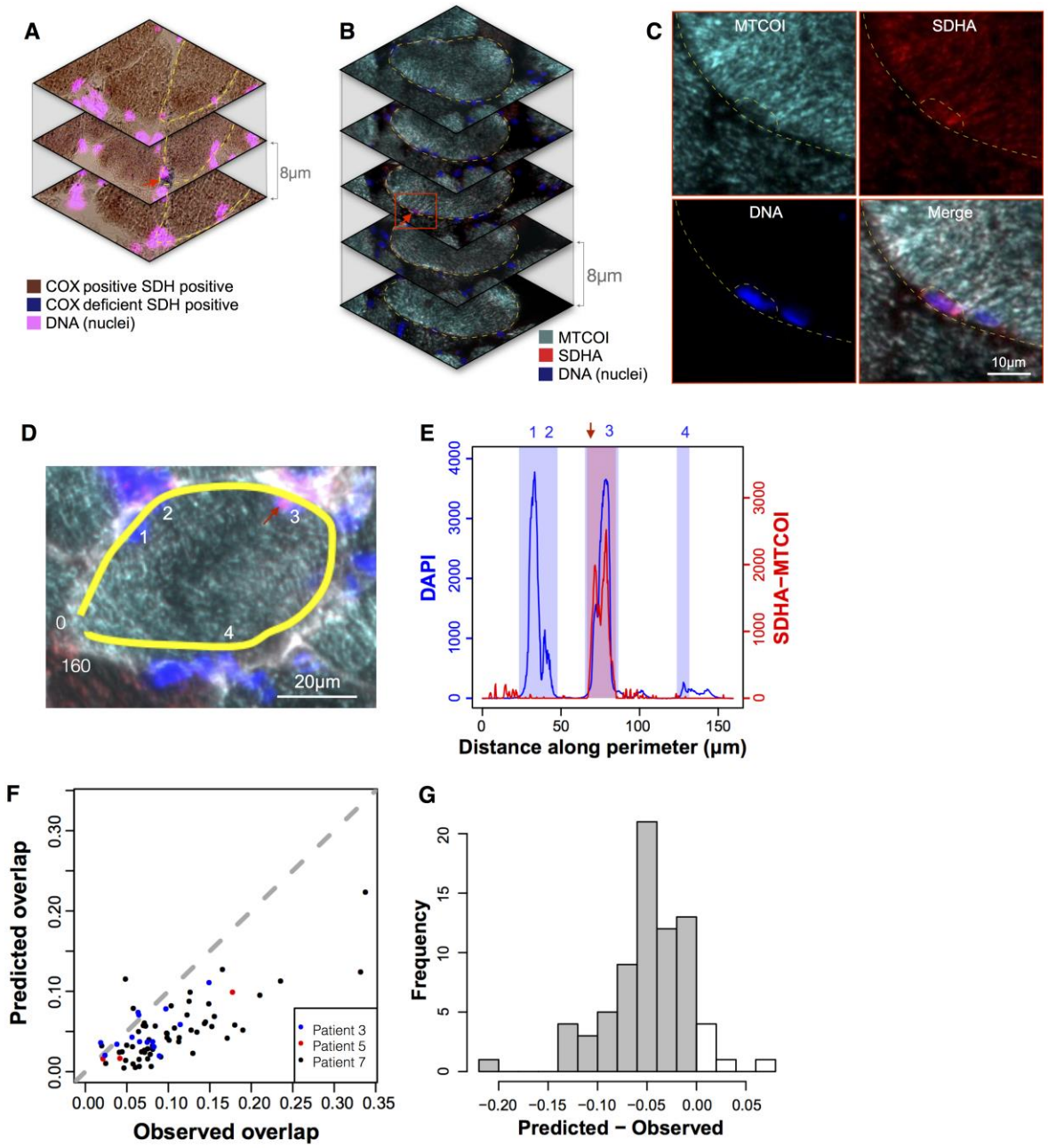

Figure 4. Foci of COX-deficient mitochondria are located in the subsarcolemmal region and colocalize with myonuclei

(A-C) Serial cryosections from patient 7 with recessive *POLG* mutations, (A) reacted for sequential COX/SDH histochemistry and DAPI and (B) labelled by triple immunofluorescence for MTCOI, SDHA, and DAPI. Note the foci of COX deficiency in the outlined cell restricted to the middle section (red arrow), indicating that the foci is less than 8um in length. (C) Magnified area from (B) showing selective absence of MTCOI staining in the perinuclear niche area outlined.

(D) An example muscle fiber from patient 3 with recessive *RRM2B* mutations, analysed using a perimeter line scan (yellow). Nuclei are indicated with numbers and the focus with a red arrow. Line scan goes from 0 to 160µm.

(E) Arbitrary fluorescence intensity for DAPI and SDHA minus MTCOI along perimeter line scan from (D). Shaded areas represent perinuclear (blue) and COX- foci (red) used to compute the degree of overlap. Note that the COX deficient foci overlaps with nucleus 3. The same analysis was applied to all foci.

(F) Scatterplot comparing predicted and observed overlap of COX- areas and nuclei along the perimeters of muscle fibers with COX- foci. Data is from patients 3 (*RRM2B)*, 5 (*POLG*) and 7 (*POLG*). Data is expressed as fractions of total muscle fiber perimeter length. Note the distribution of data towards the right of the dotted line which represents chance level (observed = expected). Example from G and H is indicated by a red arrow.

(G) Frequency histogram of Predicted - Observed overlap fractions. n = 74, one-sample t-test, p = 4.26e-15.

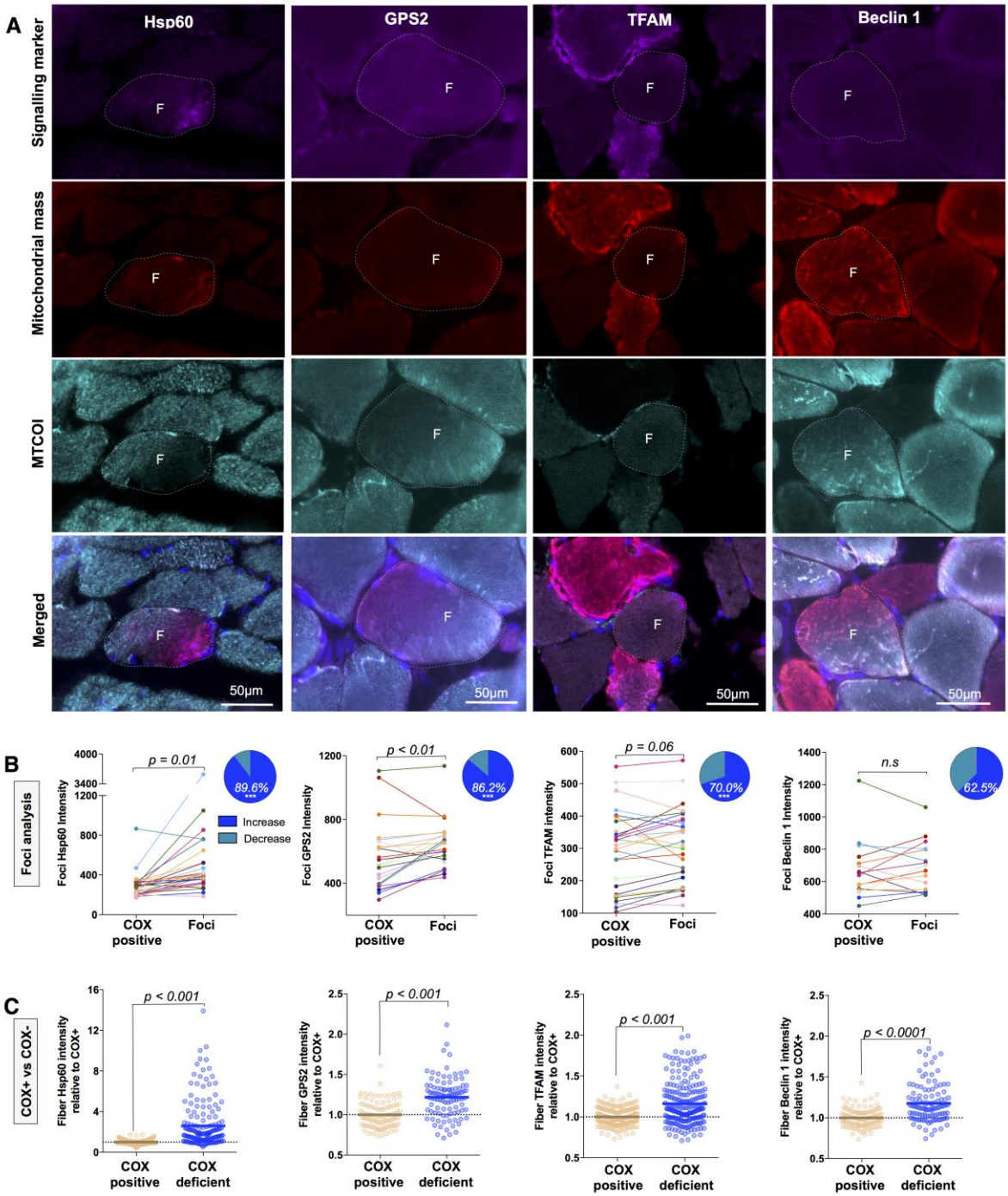

Figure 5. Activation of mito-nuclear signaling pathways in response to COX deficiency

(A) Quadruple immunofluorescent imaging of mitonuclear signaling targets Hsp60 (patient 7, *POLG)*, GPS2 (patient 5, *POLG*), TFAM (patient 7, *POLG*) and Beclin1 (patient 5, *POLG*) in combination with anti-MTCOI, anti-SDHA or anti-VDAC1 (for Hsp60) and DAPI. C indicates COX-deficient foci and yellow arrows indicate the focal region.

(B) Subcellular quantification of fluorescent intensity in COX- foci compared to COX-positive areas of the same cell from patients 3 (*RRM2B),* patient 5 *(POLG)* and patient 7 *(POLG)*. Values from the same cell are linked by a line. n = 29 (Hsp60), n = 29 (GPS2) and n= 30 (TFAM), n = 16 (Beclin1) paired t-test. Inset: Pie charts represent the percentage of foci that

have an increase in signal relative to COX-positive areas. *** $p < 0.0001$, Wilson/Brown binomial test comparing each percentage to the null hypothesis of 50:50.

(C) Whole cell fluorescent intensity in full COX+ and COX- fibers from patients 3 (*RRM2B),* patient 5 *(POLG)* and patient 7 *(POLG)*. Each data point represents a muscle fiber. n = 175 (Hsp60), n = 101 (GPS2,), n = 230 (TFAM), n = 112 (Beclin1), Mann-Whitney test).

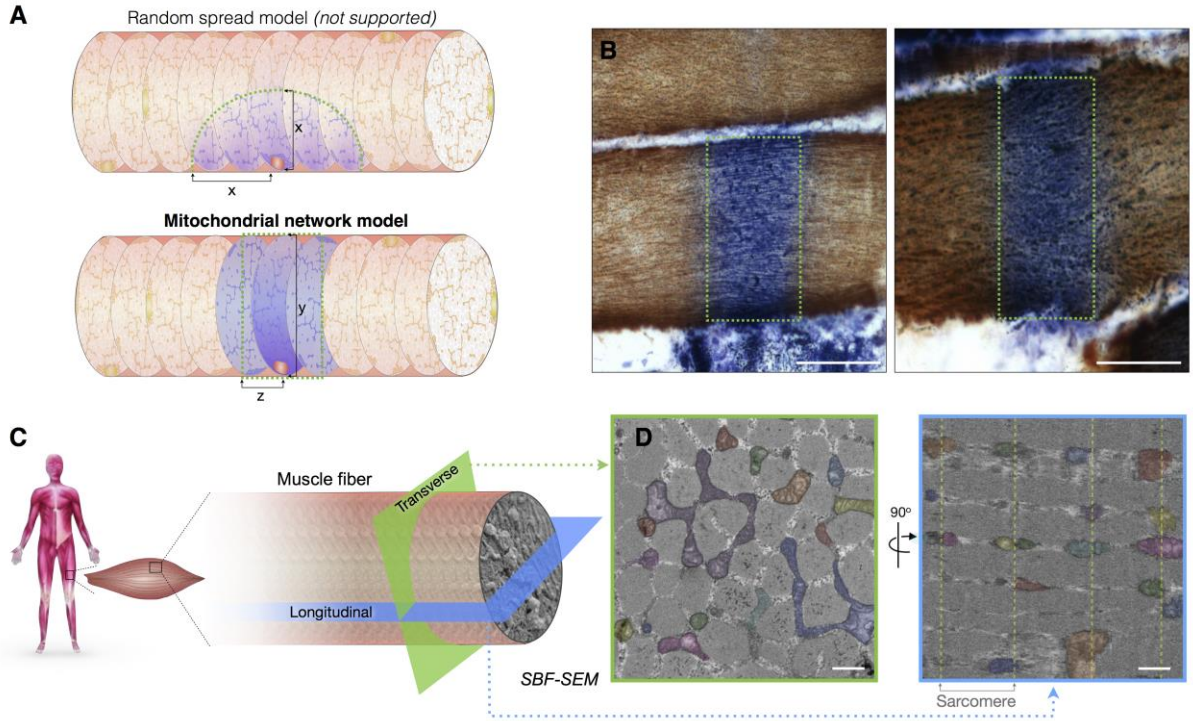

Figure 6. Sub-cellular patterns of COX deficiency and preferential transverse mitochondrial network connectivity in human muscle

(A) Hypothetical models illustrating potential spread of COX-deficient SDH positive (COX-SDH+) foci. In the random spread model (top), biochemical deficiency covers an equal distance (x) in both transverse and longitudinal orientations. In the mitochondrial network model (bottom), COX negativity can cover the width of the muscle fiber, a distance (y) that is greater than the distance covered in the longitudinal axis of the fiber (z). Dotted green boxes denote edges of biochemical deficiency.

(B) Images of thin longitudinal regions of COX-deficient segments in COX/SDH histochemistry, supporting the mitochondrial network model.

(C) Schematic demonstrating differences in mitochondrial network connectivity when examining a muscle fiber in transverse or longitudinal orientation.

(D) Results from serial block face scanning electron microscopy (SBF-SEM) showing that in the transverse orientation (green), mitochondria form an interconnected network. In the longitudinal orientation (blue), mitochondria appear round and isolated, with few connections across sarcomeres. Each continuous mitochondrion is pseudocolored, and Z-lines are marked by dotted lines.

Scale bars histochemistry (B), 50μm; scale bars electron microscopy (D), 1μm.

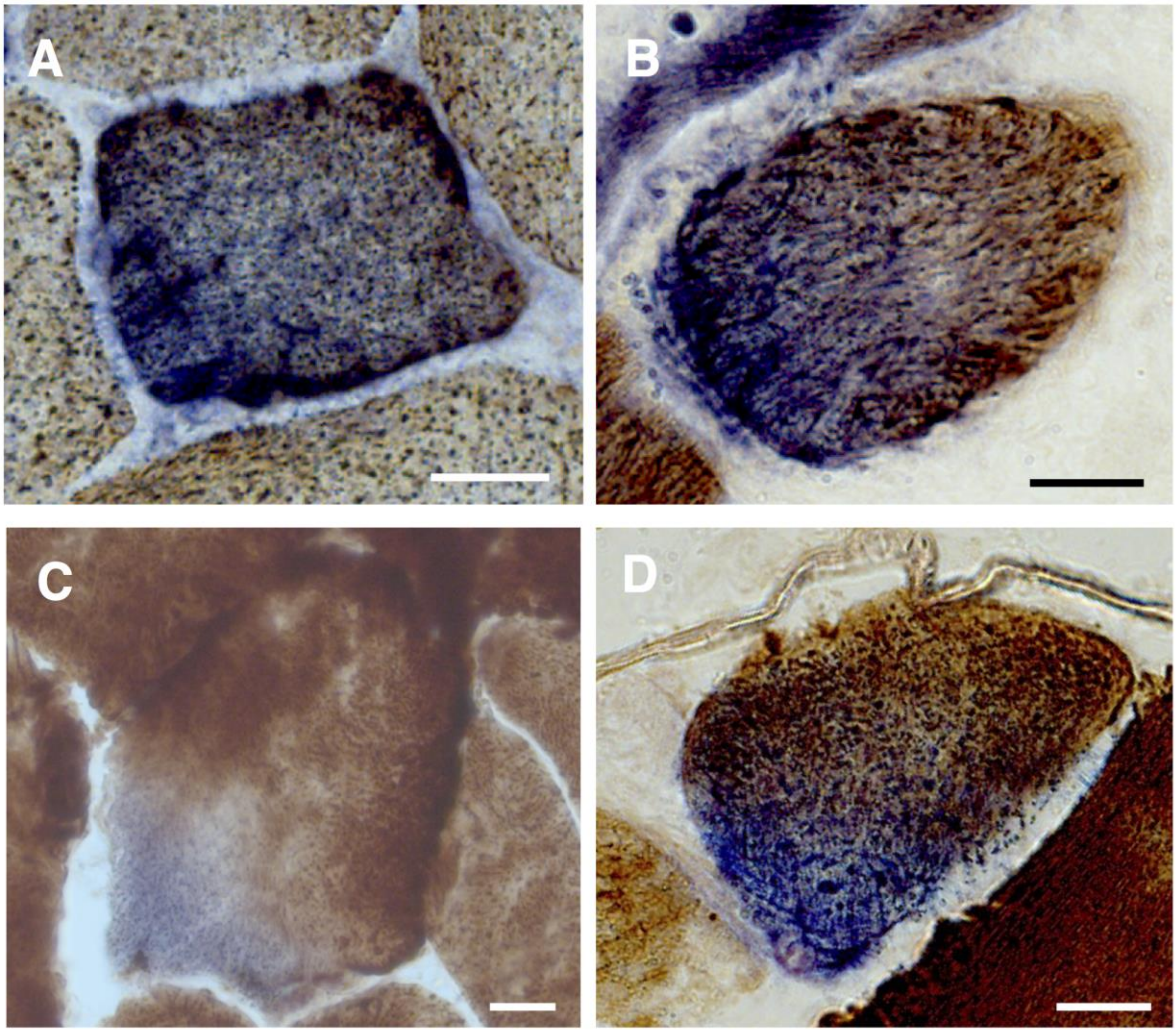

Figure 7. Foci identified in other neuromuscular diseases and ageing from COX/SDH histochemistry.

Focal COX-deficient SDH-positive region in cross-section from cases of (A) single, large scale mtDNA deletion, (B) inclusion body myositis (IBM), (C) mechanically-ventilated diaphragm and (D) normal ageing skeletal muscle.

Scale bars, 25 μm.